An air flow sensor for neonatal mechanical ventilation applications based on a novel fiber-optic sensing technique

L. Battista, S. A. Sciuto, and A. Scorza

Citation: Rev. Sci. Instrum. **84**, 035005 (2013); doi: 10.1063/1.4798298
View online: http://dx.doi.org/10.1063/1.4798298
View Table of Contents: http://rsi.aip.org/resource/1/RSINAK/v84/i3
Published by the American Institute of Physics.

An air flow sensor for neonatal mechanical ventilation applications based on a novel fiber-optic sensing technique

L. Battista,[a] S. A. Sciuto, and A. Scorza
Department of Engineering, ROMA TRE University, via della Vasca Navale 79/81, Rome, Italy

(Received 14 December 2012; accepted 11 March 2013; published online 29 March 2013)

In this work, a simple and low-cost air flow sensor, based on a novel fiber-optic sensing technique has been developed for monitoring air flows rates supplied by a neonatal ventilator to support infants in intensive care units. The device is based on a fiber optic sensing technique allowing (a) the immunity to light intensity variations independent by measurand and (b) the reduction of typical shortcomings affecting all biomedical fields (electromagnetic interference and patient electrical safety). The sensing principle is based on the measurement of transversal displacement of an emitting fiber-optic cantilever due to action of air flow acting on it; the fiber tip displacement is measured by means of a photodiode linear array, placed in front of the entrance face of the emitting optical fiber in order to detect its light intensity profile. As the measurement system is based on a detection of the illumination pattern, and not on an intensity modulation technique, it results less sensitive to light intensity fluctuation independent by measurand than intensity-based sensors. The considered technique is here adopted in order to develop two different configurations for an air flow sensor suitable for the measurement of air flow rates typically occurring during mechanical ventilation of newborns: a mono-directional and a bi-directional transducer have been proposed. A mathematical model for the air flow sensor is here proposed and a static calibration of two different arrangements has been performed: a measurement range up to 3.00×10^{-4} m^3/s (18.0 l/min) for the mono-directional sensor and a measurement range of $\pm 3.00 \times 10^{-4}$ m^3/s (±18.0 l/min) for the bi-directional sensor are experimentally evaluated, according to the air flow rates normally encountered during tidal breathing of infants with a mass lower than 10 kg. Experimental data of static calibration result in accordance with the proposed theoretical model: for the mono-directional configuration, the coefficient of determination r^2 is equal to 0.997; for the bi-directional configuration, the coefficient of determination r^2 is equal to 0.990 for positive flows (inspiration) and 0.988 for negative flows (expiration). Measurement uncertainty δQ of air flow rate has been evaluated by means of the propagation of distributions and the percentage error in the arrangement of bi-directional sensor ranges from a minimum of about 0.5% at −18.0 l/min to a maximum of about 9% at −12.0 l/min. © *2013 American Institute of Physics*. [http://dx.doi.org/10.1063/1.4798298]

I. INTRODUCTION

Flow measurements in infant mechanical ventilation and spirometry are carried out for the assessment of respiratory functions,[1] for the monitoring of air flows supplied by an infant ventilator to support neonates in intensive care units,[2,3] for the evaluation of lung ventilators performances and efficiency[4–6] and for prevention of lung injuries caused by mechanical ventilation.[7,8] Currently, various technologies are used to measure air flow in mechanically ventilated infants:[9–12] mainly employed measuring system are pneumotachographs and other transducers based on differential pressure sensing techniques, hot wire anemometers, turbine and ultrasonic flow meters, and sensors based on drag force detection performed, as example, by means of electrical strain gauge. However, in the last years, several fiber-optic sensing techniques have been proposed for medical application;[13–15] they are characterized, with respect to the traditional above quoted measurement systems based on electromagnetic or electrical working principles, by immunity to electromagnetic interferences (EMI) and by electrical insulation.[16] These last mentioned features of the fiber-optic sensors can be useful to manufactures, during design and construction of medical equipments, in order to reduce the effects due to EMI and to improve electrical safety conditions.

Despite several optical fiber sensors (OFS) for flow measurement have been recently proposed (e.g., water[17–19] and air flow[20] measurements based on the vortex shedding from optical fiber; liquid flowmeters based on fiber Bragg gratings[21–24] (FBGs), on the Coriolis measuring principle,[25] on intensity modulation of light transmitted through the optical fiber due to bending loss[26,27] and micromachined sensors for low flow measurement[28]), it is difficult to find an exhaustive investigation dealing with design and testing of optical fiber air flow meters in neonatal ventilation applications. Furthermore, proposed air flowmeters based on FBGs require interrogators or optical spectrum analyzers that are expensive and characterized by a wavelength scanning speed usually quiet limited;[16] however, their measuring technology is not affected by optical power fluctuations. On the other hand, proposed air flowmeters based on light intensity modulation are low-cost and generally characterized by a simple set-up; nevertheless,

[a]Author to whom correspondence should be addressed. Electronic addresses: luigi.battista@uniroma3.it and ing.luigi.battista@gmail.com

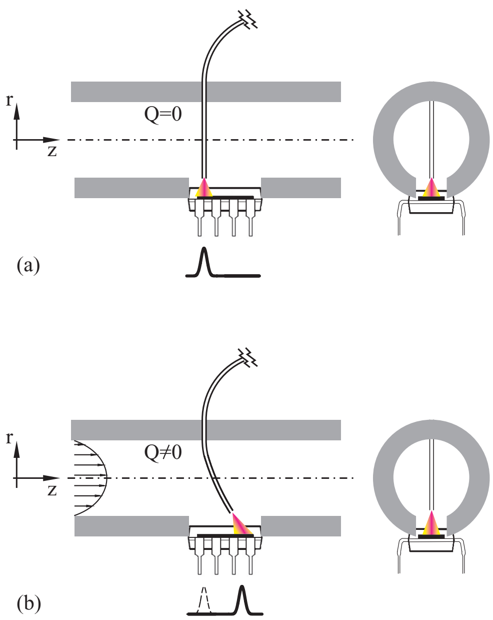

FIG. 1. Optical fiber flow sensor scheme: (a) the light from the emitting fiber hits the photodiode array, built on an integrated circuit. At null flow rate, the maximum light intensity emitted has a reference position corresponding to the maximum signal from the photodiodes; (b) as well as the flow rate Q changes, the emitting fiber bends and consequently the maximum moves from its reference position along the array direction.

they are affected by light source fluctuations independent of air flow. In this work, a simple and low-cost fiber-optic air flow sensor, based on a novel technique allowing the immunity to light intensity variations independent of air flow, has been developed for monitoring air flows supplied by a neonatal ventilator to support infants in intensive care units. The proposed flow sensor is intended to be used for monitoring air flow rate inside the ventilator (e.g., at the delivery channel).

The principle of operation of the here proposed sensor is based on the measurement of transversal displacement of an emitting fiber-optic cantilever due to action of air flow acting on it (Figure 1(a)). A similar approach was proposed for an intensity-based liquid flow sensor,[29] where the tip of the input fiber has been placed in front of an output fiber: liquid flow moves the input fiber, changing the amount of light intensity coupled to the output fiber, and, consequently, causes the variation of light intensity at the output fiber; light intensity variation is then related to flow. However, light intensity variations could be also due to the instability of light source, to the time drift of the characteristics of the optical component of the measurement system and to the losses caused by optical fiber bending and, consequently, these optical power fluctuations could be confused with an apparent flow. In the here described OFS, a novel fiber-optic sensing technique is proposed in order to achieve immunity to light intensity variations independent by measurand (in this case, the air flow): the fiber tip displacement is measured by means of a photodiode linear array, placed in front of the entrance face of the emitting optical fiber in order to detect its light intensity profile. The illumination pattern, detected by photodiode linear array, has a maximum light intensity value[30] that shifts according to the variation in flow rate (Figure 1(b)): therefore, the position of the most lighted photodiode of the linear array is related to air flow rate. The proposed measurement principle allows to directly encode the sensed information (in this case, the air flow) into an intensity distribution profile and its maximum value, which does not depend on the total light level (as long as the detected light intensity is over the noise level) and on light intensity fluctuations. Consequently, if light intensity varies during a constant flow rate, the maximum intensity value of illumination pattern changes, but the position of the most lighted photodiode of the linear array remains practically unchanged, confirming the independence of the measured flow on light intensity fluctuations. Moreover, typical flow sensors used for flow measurement in neonatal ventilation are heated (e.g., Fleisch pneumotachographs) or have a low thermal mass in order to prevent the worsening of accuracy due to water condensation caused by the humidified air; instead, the sensing principle of the proposed measurement system is characterized by immunity to light intensity variations and, therefore, can prevent the worsening of the device accuracy due to condensation.

In this work, the proposed fiber-optic sensing techniques has been used in order to develop two different arrangements of a sensor for monitoring air flow supplied by a mechanical ventilator to support infants in intensive care units: respectively, a mono-directional and bi-directional optical fiber air flow sensor for neonatal ventilation applications have been developed and are here described.

II. SENSOR STRUCTURE AND MEASUREMENT PRINCIPLE

The measurement system (Figure 2) is based on an emitting optical fiber cantilever transversally placed in a circular tube of inner radius R_f in which air mass supplied by an infant ventilator flows. The emitting fiber, with a length L, is fixed to its upper extremity and, instead, its lower extremity is free to move and is placed in front of the sensitive surface of photodiode linear array. Finally, a thin flat target disk, with radius R_D, is placed in the middle of optical fiber cantilever and perpendicular to the air flow direction. Flowing air produces a fluid drag force on the optical fiber and on the flat target disk, causing the bending of emitting optical fiber; consequently, the fiber tip displaces of a quantity measured by means of a photodiode linear array, whose axis is approximately aligned with the displacement direction. The air flow rate is then evaluated from the position of the most lighted photodiode on the array.

The mathematical relationship between the displacement Δ_{TOT} measured by photodiode linear array and air flow Q can be found by considering the equation for the wedge beam bending (optical fiber can be modeled as a cantilever beam) and the propagation of light in the gap between the fiber tip and the sensitive surface of photodiode array, that is hit by the light coming out from the emitting optical fiber (Figure 3),

$$\Delta_{TOT} = \Delta + \Delta_{gap} = \Delta + \Delta_1 + \Delta_2, \tag{1}$$

where Δ is the fiber tip displacement due to the fluid drag force acting on the fiber and target disk. The gap, constituted by two layers, provides a further amount Δ_{gap}: the first

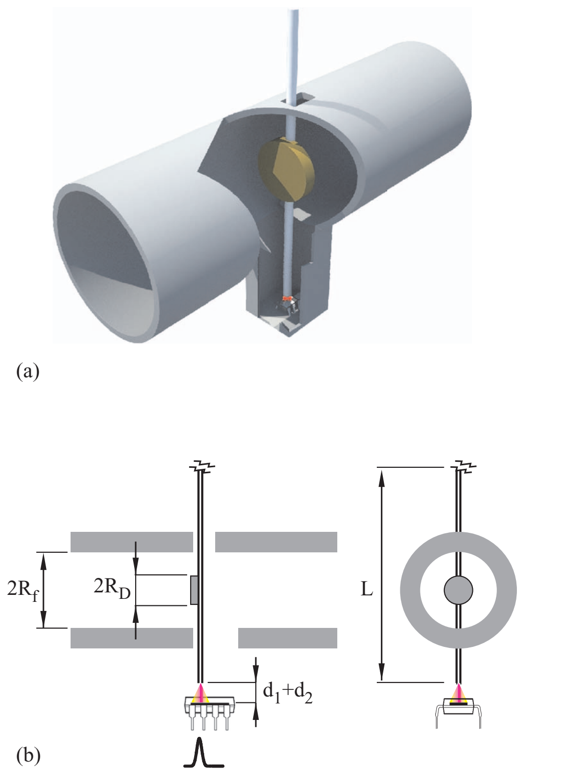

FIG. 2. Scheme of optical fiber flow sensor with main dimensions (not in scale). Mono-directional sensor: $R_f = 10$ mm; $R_D = 5$ mm; $L = 55$ mm; $d_1 = 0.5$ mm; $d_2 = 0.7$ mm. Bi-directional sensor: $R_f = 10$ mm; $R_D = 3$ mm; $L = 50$ mm; $d_1 = 0.5$ mm; $d_2 = 0.7$ mm.

sheet is an air layer (thickness d_1, refractive index $n_{air} = n_1 = 1.00$) placed between the tip of the fiber and the external packaged surface of the photodiode linear array and causes a displacement Δ_1; the second is a layer of nonconductive plastic[31] (thickness $d_2 = 0.7$ mm, refractive index $n_2 = 1.55$ at 25 °C) placed onto the sensitive surface of photodiodes of the array and causes a displacement Δ_2. The various displacement contributions are derived in Subsections II A and II B.

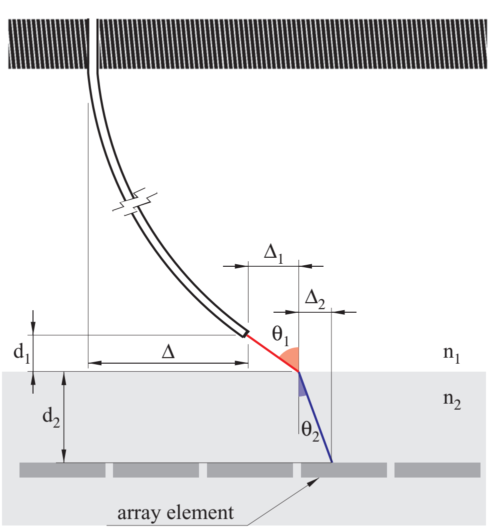

FIG. 3. Scheme for the evaluation of total displacement Δ_{TOT} measured by photodiode array.

A. Relationship between fiber tip displacement Δ and air flow Q

The mathematical relationship between the fiber tip displacement Δ and the air flow Q can be found from the equation for the wedge beam bending; even if cantilever is subjected to a distributed load due to dynamical pressure on the fiber and on the target disk, it is possible to perform a simplification by considering only the concentrated load due to fluid drag force acting on the flat target disk. In fact, preliminary numerical simulations and experimental trials have been performed considering an optical fiber, without the target disk and a distributed load: results showed that the considered arrangement (shown in Figure 1) is not enough sensitive to detect small fiber tip displacements, due to resolution of photodiodes linear array[31] (400 dots per inch) that allows a minimum detectable displacement equal to 63.5 μm. On the other side, as described in Sec. IV, the measurement system with target disk is able to detect displacements up to about 7 mm for air flow rates up to 18.0 l/min (3.00×10^{-4} m^3/s), which are flow rates normally encountered during neonatal ventilation in infants[32] with a maximum mass of 10 kg. Therefore, it is possible to neglect the effects due to distributed load on the fiber, because they produce a displacement lower than minimum detectable displacement (63.5 μm) and much lower than ones due to concentrated load constituted by the thin flat target disk (up to about 7 mm). Thus, an approximated relationship between the fiber tip displacement Δ and the air flow Q can be found from the equation for the wedge beam bending with a concentrated load F in the middle of the optical fiber cantilever,[33]

$$\Delta = \frac{F \cdot L^2}{6 \cdot E \cdot I} \cdot (3 \cdot L - x_F) \cong \frac{5}{48} \cdot \frac{F \cdot L^3}{E \cdot I}, \tag{2}$$

where $x_F = L/2$ is the position, respect to the wedge, where the load F is concentrated, E is the Young modulus ($E = 4.34$ GPa for an optical fiber with polymer coating and $E = 71.8$ GPa for an uncoated silica fiber[34]), and I is the momentum of inertia of the circular fiber[35] with an outer diameter D_f,

$$I = \frac{\pi \cdot D_f^4}{64}. \tag{3}$$

As in the described scenario (i.e., air flow, up to 18 l/min, at room temperature in a tube of diameter of 20 mm) the maximum Reynolds number is about 1300, laminar flow occurs; consequently, the mathematical relationship, between the air flow rates Q, and the concentrated load F on the flat target disk, can be found considering the velocity distribution v_z in the laminar flow,

$$v_z(r) = v_{z,max} \cdot \left(1 - \left(\frac{r}{R}\right)^2\right) \tag{4}$$

with the maximum value of velocity $v_{z,max,}$ occurring in the middle of the section of tube

$$v_{z,max} = 2 \cdot V = 2 \cdot \frac{Q}{S} = 2 \cdot \frac{Q}{\pi \cdot R^2}, \tag{5}$$

where V is the mean flow velocity, r is the radial distance from the center axis of the tube in its cylindrical reference system, S is the cross-sectional area of the circular tube, and R_f is its radius. The laminar flow acting on the flat target disk causes a fluid drag force F; concentrated load F is then evaluated performing mathematical integration of the elementary drag force dF on each elementary annulus of area $2\pi \cdot r \cdot dr$ in the range $0 \le r \le R_D$,

$$F = \int_0^{R_D} C_D \cdot \left(\frac{1}{2}\rho \cdot [v_z(r)]^2\right) \cdot 2\pi \cdot r \cdot dr, \qquad (6)$$

where ρ is the air density, dynamic pressure is the amount in round brackets, and C_D is drag coefficient for a thin flat plate perpendicular to flow. Drag coefficient C_D, which in general depends on object shape and Reynolds number, can be considered, for a thin plate perpendicular to air flow, equal to 2.0 for a wide range of Reynolds number.[36,37] Considering (4) and (5), concentrated load F can be obtained by integration of (6),

$$F = \frac{2}{3} \cdot \frac{C_D \cdot \rho}{\pi \cdot R^8} \cdot R_D^2 \cdot \left(3 \cdot R^4 - 3 \cdot R^2 \cdot R_D^2 + R_D^4\right) \cdot Q^2. \qquad (7)$$

However, by expressing air density ρ as

$$\rho = \frac{P}{R_S \cdot T}, \qquad (8)$$

where T is the absolute temperature, P is absolute pressure, RS is the specific gas constant for dry air equal to 287.058 J/(kg K) (the effects of relative humidity, in a first approximation, can be neglected), by substituting (7) and (8) in (2), the relationship between air flow rate Q and fiber tip displacement Δ is found,

$$Q = \sqrt{\frac{9\pi^2 \cdot R_S}{40} \cdot \frac{E \cdot T \cdot d_f^4 \cdot R^8}{C_D \cdot P \cdot L^3 \cdot R_D^2 \cdot \left(3 \cdot R^4 - 3 \cdot R^2 \cdot R_D^2 + R_D^4\right)}} \cdot \sqrt{\Delta} = C \cdot \sqrt{\Delta}, \qquad (9)$$

where C is a constant depending on air density ρ, drag coefficient C_D, on mechanical and dimensional characteristics of the optical fiber and on dimensional characteristics of target disk and pipe,

$$C = \left[\frac{9\pi^2}{40} \cdot \frac{E \cdot D_f^4 \cdot R^8}{C_D \cdot \rho \cdot L^3 \cdot R_D^2 \cdot \left(3 \cdot R^4 - 3 \cdot R^2 \cdot R_D^2 + R_D^4\right)}\right]^{1/2}, \qquad (10)$$

C is equal to 6.3 l min^{-1} mm$^{-1/2}$ for mono-directional configuration and 13.0 l min^{-1} mm$^{-1/2}$ for bi-directional configuration.

B. Gap contribution

The displacement Δ_{TOT} measured by means of photodiode linear array is greater than fiber tip displacement Δ due to the propagation of light in the gap between the fiber tip and the sensitive surface of photodiode array, causing an additional displacement Δ_{gap}, which is the sum of two contributions, related, respectively, to air gap and plastic gap,

$$\Delta_{gap} = \Delta_1 + \Delta_2. \qquad (11)$$

With reference to Figure 3, Δ_1 and Δ_2 can be evaluated by means of geometrical considerations

$$\Delta_1 = d_1 \cdot \tan\theta_1, \qquad (12)$$

$$\Delta_2 = d_2 \cdot \tan\theta_2, \qquad (13)$$

where θ_1 is the fiber slope at its end and can be approximated with the equation for the wedge beam bending with a concentrated load F in the middle of the optical fiber cantilever,[33]

$$\theta(Q) = \frac{F(Q) \cdot L^2}{8 \cdot E \cdot I}, \qquad (14)$$

where θ is function of air flow Q because the concentrated load F, calculated in (7) is a function of Q. The relationship between θ_1 and θ_2 is expressed by the Snell law,

$$n_1 \cdot \sin\theta_1 = n_2 \cdot \sin\theta_2 \qquad (15)$$

and can be simplified with (16) under the small angle approximation (θ_1 ranges from about 0, for a null flow, up to 0.17 rad for Q = 18 l/min),

$$\theta_2 \cong \frac{n_1}{n_2}\theta_1. \qquad (16)$$

From Eqs. (11) to (16), the displacement Δ_{gap} is

$$\Delta_{gap} = d_1 \cdot \tan\theta_1 + d_2 \cdot \tan\left(\frac{1}{n_2}\theta_1\right), \qquad (17)$$

Δ_{gap} increases when Q increases.

C. Relationship between displacement Δ_{TOT} and air flow Q

Finally, the mathematical relationship between the displacement $\Delta_{TOT} = \Delta + \Delta_{gap}$ measured by photodiode linear array and air flow Q can be evaluated by substituting (9) and (17) in (1),

$$\Delta_{TOT}(Q) = C \cdot \sqrt{Q} + \left[d_1 \cdot \tan\theta_1(Q) + d_2 \cdot \tan\left(\frac{\theta_1(Q)}{n_2}\right)\right], \qquad (18)$$

where the quantity in square bracket Δ_{gap} is the gap contribution to total displacement Δ_{TOT}. As numerical simulations predict that $\Delta_{gap} \ll \Delta$ if $d_1 < 1$ mm, gap contribution Δ_{gap} to the displacement Δ_{TOT} can be neglected (e.g., for Q = 18 l/min, d_1 = 0.500 mm, $n_1 = n_{air}$ = 1.00 and n_2 = 1.55 at 25 °C,[31] Δ is about 7.5 mm and Δ_{gap} is about 170 μm, in other terms Δ_{gap} is less than 2.3% of Δ),

$$\Delta_{TOT} = \Delta + \Delta_{gap} \cong \Delta = C \cdot \sqrt{Q}. \qquad (19)$$

As a consequence of the above mentioned assumption, the approximated relation between the displacement measured by photodiode linear array and air flow rates Q considered in the following will be Eq. (9), which is substantially identical to (19).

III. EXPERIMENTAL SETUP

With reference to the setup showed in Figure 4, experimental trials were carried out in order to perform static

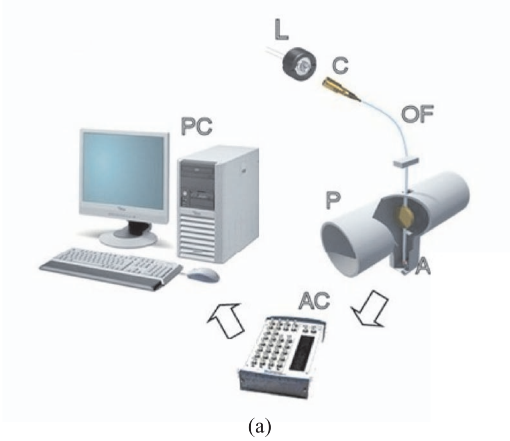

(a)

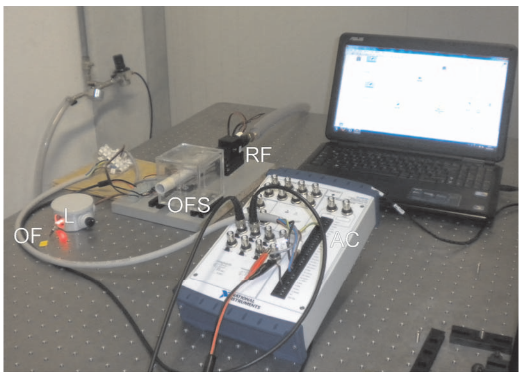

(b)

FIG. 4. (a) Schematic of experimental setup (not in scale). (b) Experimental setup. L: light emitting diode supplying optical fiber; OF: optical fiber; OFS: optical fiber air flow sensor; RF: reference air flow sensor; AC: data acquisition card; C: aspheric collimator; P: pipeline.

calibration of the device. The light emitted by an Epoxy-Encased Light Emitting Diode L (LED630E Thorlabs, 639 nm, 7.2 mW) is collimated into a 62.5/125 μm multi-mode optical fiber OF by means of an aspheric collimator C (F230FC-B Thorlabs). After propagation along coated optical fiber, light emerging from the fiber tip is projected onto the photodiode linear array A (TAOS TSL1401R-LF31, 128 pixels, 400 dots per inch, responsivity 35 V/(μJ/cm^2 . Afterward, photodiode linear array A converts the illumination pattern impinging on it into an electrical signal, which is then acquired by means of a data acquisition card AC (NI USB-6251 BNC) that subsequently sends it to a laptop PC, where it is processed in a LabVIEW environment: the position of the most lighted photodiode in the array, evaluated by means of digital data processing, is finally related to air flow rates Q. Digital output module of AC is also used in order to generate Serial Input signal (SI), allowing the temporization of consecutive array scans (single scan duration of 206.4 μs, sampling frequency of 25 scans/s, allowing a time resolution of 40 ms for the proposed optical fiber flow sensor).

Furthermore, the distance between the fiber tip and the array packaged surface is set to 500 μm by means of a travel stage (NF5P1/M Thorlabs) which provides a resolution of 1 μm. Experimental trials have been performed for different air flow rates (as maximum Reynolds number is about 1300, laminar flow occurs) set by adjusting the output pressure from

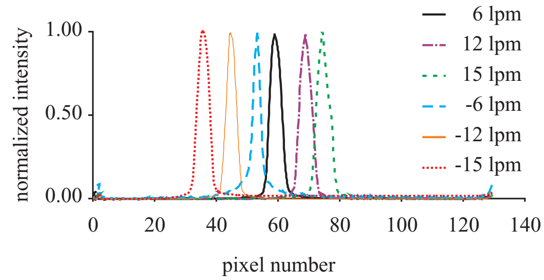

FIG. 5. Measurements results for bi-directional flow sensor: detected illumination patterns for different air flow values.

a compressor as long as the output of a reference air flow sensor RF (Honeywell AWM5104, 0.1–20 l/min, accuracy of 3%) indicates the established input air flow value.

IV. RESULTS

In order to obtain the static calibration of two proposed configurations of optical fiber air flow sensor, the experimental setup shown in Figure 4 has been used. Measurements were conducted up to 3.00×10^{-4} m^3/s (18.0 l/min), i.e., flow range normally encountered[32] during tidal breathing of infants with a mass lower than 10 kg, in step of 5.0×10^{-5} m^3/s (3.0 l/min); air flow rates have been set by adjusting the working pressure of the compressor as long as the output of reference air flow sensor RF indicates the established air flow rate. Intensity distribution profiles, measured for different air flow values and measured by means of the photodiode linear array during static calibration of bi-directional air flow sensor, are shown in Figure 5; afterward, the position of the most lighted photodiode in the array, evaluated by means of digital data processing, is related to the set air flow rates Q, as shown in Figure 6.

Experimental and theoretical relationship between the fiber tip displacement Δ and air flow Q are displayed in Figure 6: in the arrangement of mono-directional air flow sensor the coefficient of determination is $r^2 = 0.997$; in the arrangement of bi-directional air flow sensor the coefficient of determination is $r^2 = 0.990$ for positive flows (inspiration) and is $r^2 = 0.988$ for negative flows (expiration): in each configuration a good agreement between experimental data and the mathematical model, expressed by (19), can be deduced. Moreover, Figure 6 shows that keeping to a constant value the radius of the pipe R_f (20 mm) and varying the size of the disk R_D (from 10 mm to 6 mm) the sensitivity of the device varies, as expected by (9). Results show that the lower limit of the measuring interval is 2.0 l/min and 3.0 l/min, respectively, for mono-directional and bi-directional configuration due to the resolution of the photodiode array that allows a minimum detectable displacement equal to 63.5 μm.

V. EVALUATION OF UNCERTAINTY

An evaluation of measurement uncertainty in the calibration range and for both configurations has been performed according to the propagation of distribution (as indicated in "Supplement 1 to the Guide to the expression of uncertainty

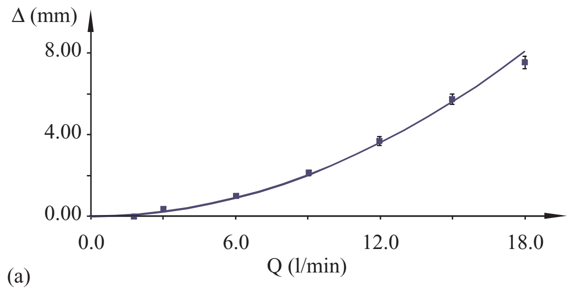

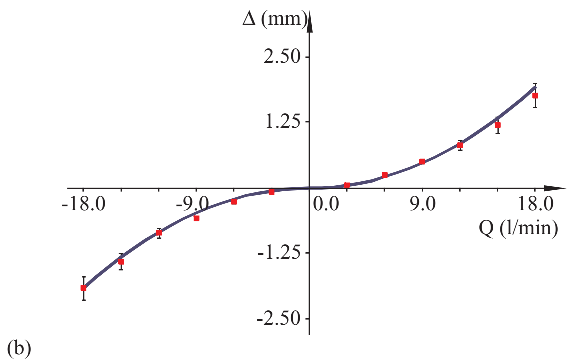

FIG. 6. Measurements results: displacement Δ as a function of flow rate Q. (a) mono-directional air flow sensor; (b) bi-directional air flow sensor.

in measurement"[38]) by means of the Monte Carlo method (MCM). The theoretical model describes air flow rate Q (quantity not directly measured), as a function of different inputs,

$$Q = Q(E, T, P, d_f, R, C_D, L, R_D, \Delta) \tag{20}$$

and mathematical relationship can be expressed by (9). According to the propagation of distributions,[38] on the basis of the available knowledge, probability density functions (PDFs) have been assigned to the independent input quantities and then these PDFs have been propagated through the model (19) to obtain the PDF for the air flow rate Q, from which the expectation value and the shortest 95% coverage interval for Q [l/min] have been derived. The direct measurements (confidence level 95%) and the PDFs of the input quantities are derived as follows and summarized in Tables I and II:

- [34]Young modulus E of the polymer coated optical fiber has been considered equal to 4.3 GPa with an uncertainty of 5%: E = [E−δE, E+δE] = [4.1 GPa, 4.5 GPa]. In this work, E has been modeled by a normal distribution with a mean equal to 4.3 GPa and with a standard deviation σE estimated by considering that the value of the Young modulus E lies in the interval E−δE and E+δE with a 95% probability: $\sigma_E = \delta E/(1.96)$;
- Air temperature T has been measured with a K type thermocouple IsoTech ITA11 (accuracy: 0.5% + 2 K): T ± δT = (295 ± 2) K; T has been described by a Gaussian PDF with a mean equal to 295 K and with a standard deviation σT estimated by considering that the value of the air temperature lies in the interval T−δT to T+δT with a 95% probability: $\sigma_T = \delta T/1.96$;

TABLE I. PDFs assigned to the input quantities in order to perform the propagation of distribution. N(μ, σ) is a Gaussian PDF with mean m and standard deviation σ; U(μ, σ) is a uniform PDF with mean m and standard deviation σ.

Quantity	PDF	Parameters m	Parameters σ
E	N(m, σ)	4.3 GPa	0.1 Gpa
T	N(m, σ)	295.0 K	0.5 K
P	U(m, σ)	101 kPa	6 kPa
D_f	N(m, σ)	245 μm	4 μm
R	U(m, σ)	1.000 cm	0.003 cm
C_D	N(m, σ)	2.00	0.06
L	U(m, σ)	5.60 cm	0.03 cm
R_D	U(m, σ)	6.00 mm	0.03 mm

- [32]As the pressure normally encountered during pulmonary function tests in infants and young children ranges from −10 kPa to 10 kPa, an uniform PDF with a lower limit of −10 kPa and an upper limit of 10 kPa has been assigned to the absolute pressure P;
- The outer diameter of the optical fiber, in accordance to the MM625 datasheet, is $D_f \pm \delta D_f = (245 \pm 7)$ μm; for the propagation of distribution, D_f has been modeled by a normal PDF with a mean equal to 245 μm and with a standard deviation σ_{Df} estimated by considering that the value of the outer diameter lies in the interval $D_f - \delta D_f$ to $D_f + \delta D_f$ with a 95% probability: $\sigma_{Df} = \delta D_f/1.96$;
- The drag coefficient for a thin flat plate perpendicular to flow has been considered equal to $C_D \pm \delta C_D = 2.0 \pm 0.1$, as indicated by Lisosky[37] and Hoerner;[36] C_D has been modeled by a Gaussian distribution with a mean equal to 2.0 and with a standard deviation σ_{CD} estimated by considering that the value of the drag coefficient C_D lies in the interval 1.9–2.1 with a 95% probability: $\sigma_{CD} = \delta C_D/1.96$;
- Uniform PDFs have been assigned to describe length measurements: the length of the fiber L has been measured with a resolution of 1 mm; both the radius of the tube R and the radius of the circular disk target R_D have been derived from the measurement of the respective diameters by means of a decimal caliper;

TABLE II. Mono-directional configuration of air flow sensor: PDFs assigned according to independent displacements detected by means of the photodiode array. N(μ, σ) is a Gaussian PDF with mean m and standard deviation σ; U(μ, σ) is an uniform PDF with mean m and standard deviation σ.

Q_{set} (l/min)	PDFs displacement Δ (mm)
2.0	U(m = 0.60 mm, σ = 0.02 mm)
3.0	U(m = 0.19 mm, σ = 0.02 mm)
6.0	U(m = 1.02 mm, σ = 0.02 mm)
9.0	N(m = 2.15 mm, σ = 0.06 mm)
12.0	N(m = 3.71 mm, σ = 0.11 mm)
15.0	N(m = 5.75 mm, σ = 0.13 mm)
18.0	N(m = 7.54 mm, σ = 0.15 mm)

TABLE III. Bi-directional configuration of air flow sensor: PDFs assigned according to independent displacements detected by means of the photodiode array. N(μ, σ) is a Gaussian PDF with mean μ and standard deviation σ; U(μ, σ) is an uniform PDF with mean μ and standard deviation σ.

Q_{set} (l/min)	PDFs positive displacement Δ	PDFs negative displacement Δ
±3.0	U(0.06 mm, 0.02 mm)	U(−0.06 mm, 0.02 mm)
±6.0	U(0.25 mm, 0.02 mm)	U(−0.25 mm, 0.02 mm)
±9.0	U(0.51 mm, 0.02 mm)	U(−0.57 mm, 0.02 mm)
±12.0	N(0.82 mm, 0.04 mm)	N(−1.02 mm, 0.04 mm)
±15.0	N(1.21 mm, 0.08 mm)	N(−1.40 mm, 0.08 mm)
±18.0	N(1.78 mm, 0.11 mm)	N(−1.91 mm, 0.11 mm)

- The displacement Δ and its uncertainty $\delta\Delta$, have been derived by a statistical analysis of the measurements, performed with the photodiode array, at different air flow rates Q (Figure 8). The PDFs of the displacement, derived from multiple independent observations, are summarized in Tables II and III, respectively, for mono-dirctional and bi-directional configuration.

Finally, the measurement uncertainty δQ in the calibration range takes into account of the accuracy of the reference sensor (Honeywell AWM5104, 0.1–20 l/min, 3% accuracy).

Table II shows a constant displacement uncertainty at low flow rates (up to 6.0 l/min): from a series of independent observations, the most illuminated photodiode in the array is the same, as shown in Figure 7(a), and so the displacement uncertainty is estimated by assuming a rectangular probability distribution (type B evaluation of standard uncertainty[39]) with a width equal to photodiode longitudinal dimension (63.5 μm). For air flows greater than 6.0 l/min, the most illuminated photodiode in the array is not the same due to the fluctuation of optical fiber caused by vortex shedding: the considered fiber fluctuation exists also for air flows lower than 6.0 l/min, but the amplitude of fluctuation is lower than resolution allowed by photodiode array; for air flows greater than 6.0 l/min, the amplitude of vibration (caused by vortex shedding occurring at higher flow values) increases and becomes greater than resolution of the photodiode array. As consequence, for air flows greater than 6.0 l/min a series of independent observations of displacement provides a normal distribution, as shown in Figure 7(b): Δ value is calculated by averaging a series of independent observations of displacements, and $\delta\Delta$ can be evaluated from multiplying the standard deviation of the mean by the coverage factor associated with a level of confidence of 95% (type A evaluation of standard uncertainty[39]).

Uncertainty values for the air flow rate are evaluated by means of the propagation of the PDFs[38] (implemented in a MATLAB environment through the MCM with a number of trials equal to 10^6 according to Supplement[38]) and are compared in Tables IV–VI; the PDFs of air flow rate evaluated through the propagation of distributions are shown in Figure 8. Tables IV–VI show also the percentage error $\varepsilon_{\%}$ as expressed in (21),

$$\varepsilon_{\%} = \frac{|Q_{set} - Q|}{Q_{set}} \cdot 100\%, \tag{21}$$

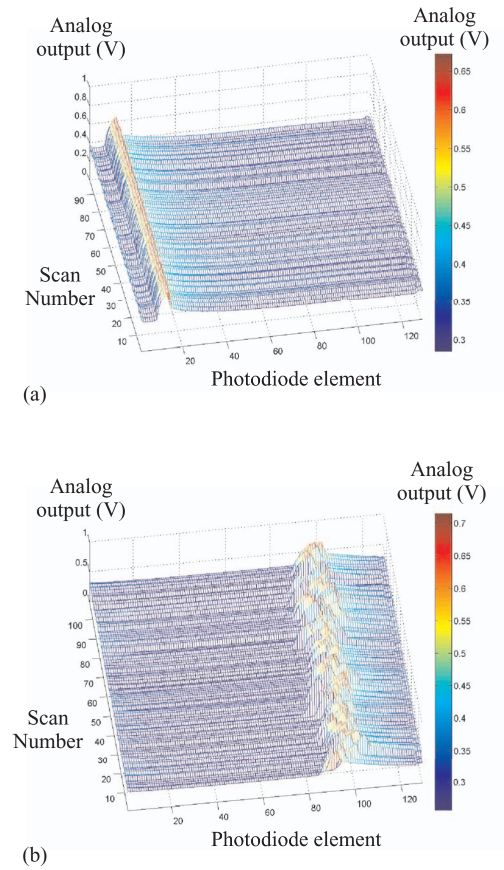

FIG. 7. Intensity distribution profiles for two different air flow values. (a) Low air flow rate of 3 l/min: illumination patterns have their maximum in correspondence of the same photodiode of the array (on 98 different scans the most illuminated photodiode, is the element number 10). (b) High air flow rate of 15 l/min: illumination patterns have their maximum in correspondence of different photodiodes, as well as on 109 different scans, the most illuminated photodiode, shifts between the element number 90 and the element number 103.

where Q_{set} is the air flow value measured by the reference sensor and Q is the flow evaluated by substituting the measured displacement Δ in the theoretical model (19).

Results of propagation of distributions implemented by means of MCM show that measurement uncertainty tend to increases with Q; this phenomenon can be ascribed to fiber fluctuation caused by vortex shedding occurring mainly at higher flow values. Results also show that the percentage error

TABLE IV. Mono-directional configuration of air flow sensor: shortest coverage interval and percentage error ε% of Q, evaluated by means of the propagation of distributions (MCM).

Q_{set} (l/min)	Mean value for Q (l/min)	Shortest 95% coverage interval for Q (l/min)	$\varepsilon_{\%}$ (%)
2.0	2.2	[1.7, 2.8]	10
3.0	2.8	[2.2, 3.3]	6.7
6.0	6.4	[5.7, 7.2]	6.7
9.0	9.3	[8.3, 10.4]	3.3
12.0	12.3	[11.0, 13.6]	2.5
15.0	15.3	[13.7, 16.8]	2.0
18.0	17.5	[15.8, 19.2]	2.8

TABLE V. Positive displacements of bi-directional configuration of air flow sensor: shortest coverage interval and percentage error $\varepsilon_{\%}$ of Q, evaluated by means of the propagation of distributions (MCM).

Q_{set} (l/min)	Mean value for Q (l/min)	Shortest 95% coverage interval for Q (l/min)	$\varepsilon_{\%}$ (%)
3.0	3.1	[2.1, 4.1]	4.8
6.0	6.5	[5.7, 7.3]	8.1
9.0	9.3	[8.3, 10.4]	3.5
12.0	11.8	[11.5, 13.1]	1.4
15.0	14.4	[12.7, 16.1]	4.4
18.0	17.4	[15.4, 19.5]	3.3

TABLE VI. Negative displacements of bi-directional configuration of air flow sensor: shortest coverage interval and percentage error $\varepsilon_{\%}$ of Q, evaluated by means of the propagation of distributions (MCM).

Q_{set} (l/min)	Mean value for Q (l/min)	Shortest 95% coverage interval for Q (l/min)	$\varepsilon_{\%}$ (%)
−3.0	3.1	[2.1, 4.1]	4.8
−6.0	6.5	[5.7, 7.4]	8.1
−9.0	9.8	[8.8, 10.9]	8.7
−12.0	13.2	[11.8, 14.6]	9.1
−15.0	15.4	[13.7, 17.3]	3.0
−18.0	18.1	[16.0, 20.1]	0.5

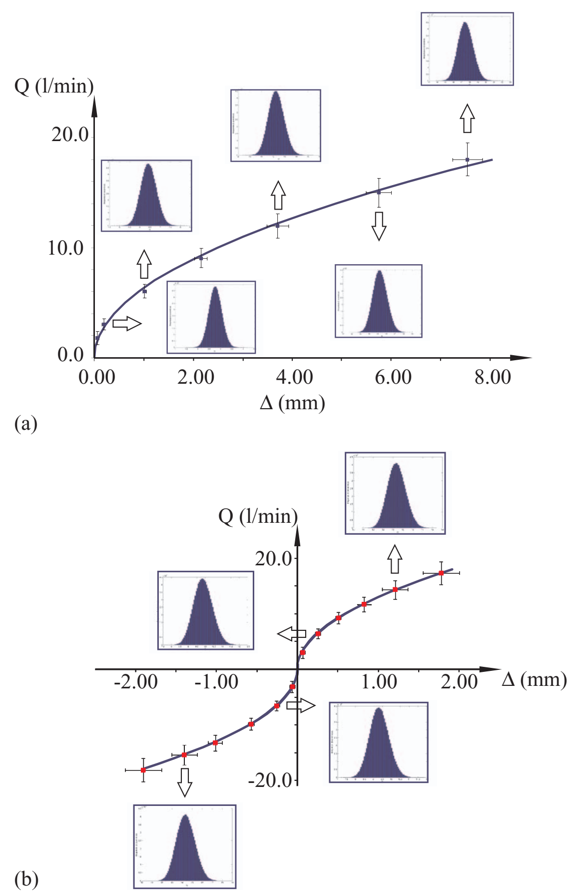

FIG. 8. Mathematical model expressed by (19), experimental data and PDFs of the air flow rate obtained through the Monte Carlo Method (MCM). (a) mono-directional configuration; (b) bi-directional configuration.

in the arrangement of mono-directional sensor ranges from a minimum of about 2% at 15.0 l/min to a maximum of about 10% at 2 l/min and the percentage error in the arrangement of bi-directional sensor ranges from a minimum of about 0.5% at −18.0 l/min to a maximum of about 9% at −12.0 l/min. In order to reduce the measurement uncertainty δQ, it would be necessary to improve the knowledge of the input quantities (e.g., performing a measurement of E, T, and P with a lower uncertainty) and to use a photodiode array with better resolution and by means of a more accurate reference sensor at low flow rate.

VI. DISCUSSION AND CONCLUSIONS

In this work, a low-cost air flow sensor, based on a novel fiber-optic sensing technique has been developed for monitoring air flows rates supplied by a neonatal ventilator to support infants in intensive care units. The device is based on a fiber optic sensing technique allowing the immunity to light intensity variations independent by measurand and allowing the reduction of typical shortcomings affecting all biomedical fields (EM interference and patient electrical safety). The sensing principle is based on the measurement of transversal displacement of an emitting fiber-optic cantilever due to action of air flow acting on it; the fiber tip displacement is measured by means of a photodiode linear array, placed in front of the entrance face of the emitting optical fiber in order to detect its light intensity profile. As the measurement system is based on a detection of the illumination pattern, and not on an intensity modulation technique, it results less sensitive to light intensity fluctuation independent by measurand than intensity-based sensors. The considered novel fiber-optic sensing technique is here used in order to develop two different configurations for an air flow sensor suitable for the measurement of air flow rates typically occurring during mechanical ventilation of newborn: a mono-directional and a bi-directional transducer have been proposed. A mathematical model for the air flow sensor has here presented and a static calibration of two different arrangements has been performed: a measurement range up to 3.00×10^{-4} m^3/s (18.0 l/min) for the mono-directional sensor and a measurement range of $\pm 3.00 \times 10^{-4}$ m^3/s (±18.0 l/min) for the bi-directional sensor have been experimentally evaluated, according to the air flow rates normally encountered during tidal breathing of infants with a mass lower than 10 kg. Experimental data of static calibration result in accordance with the proposed theoretical model: for the mono-directional configuration, the coefficient of determination r^2 is equal to 0.997; for the bio-directional configuration, the coefficient of determination r^2 is equal to 0.990 for positive flows (inspiration) and 0.988 for negative flows (expiration). Measurement uncertainty δQ of air flow rate has been evaluated by means of the propagation of distributions (implemented in a MATLAB environment through Monte Carlo method) and the percentage error in the arrangement of mono-directional sensor ranges from a minimum of about 2% at 15.0 l/min to a maximum of about 10% at 2 l/min; on the other hand, the percentage error in the arrangement of bi-directional sensor ranges from a minimum of about 0.5% at −18.0 l/min to a maximum of about 9% at −12.0 l/min.

[1] J. G. Webster and A. M. Cook, *Clinical Engineering: Principles and Practices* (Prentice-Hall, Englewood Cliffs, NJ, 1979).
[2] R. C. Bone and D. H. Eubanks, Dis Mon. **37**, 321 (1991).
[3] P. J. F. M. Merkus, J. C. de Jongste, and J. Stocks, Eur. Respir. Mon. **31**, 166 (2005).
[4] P. Cappa, S. A. Sciuto, and S. Silvestri, J. Med. Eng. Technol. **30**, 31 (2006).
[5] T. Torzala, Med. Electron. **1**, 87 (1987).
[6] P. Cappa, S. A. Sciuto, and S. Silvestri, Rev. Sci. Instrum. **73**, 2411 (2002).
[7] A. S. Slutsky, Chest **116**, 9S (1999).
[8] D. Dreyfuss and G. Saumon, Am. J. Respir. Crit. Care Med. **157**, 294 (1998).
[9] R. C. Baker, *Flow Measurement Handbook: Industrial Designs, Operating Principles, Performance, and Applications* (Cambridge University Press, Cambridge, 2000).
[10] F. P. Branca, *Fondamenti di Ingegneria Clinica* (Springer-Verlag, Milan, Italia, 2000), Vol. 1.
[11] E. Schena and S. Silvestri, Rev. Sci. Instrum. **79**, 104301 (2008).
[12] P. Saccomandi, E. Schena, and S. Silvestri, Rev. Sci. Instrum. **82**, 024301 (2011).
[13] E. Pinet, Nat. Photonics **2**, 150 (2008).
[14] P. Rolfe, S. Scopesi, and G. Serra, Meas. Sci. Technol. **18**, 1683 (2007).
[15] J. I. Peterson and G. G. Vurek, Science **224**, 123 (1984).
[16] B. Lee, Opt. Fiber Technol. **9**, 57 (2003).
[17] P. A. Leilabad, J. D. C. Jones, A. D. Kersey, M. Corke, and D. A. Jackson, Electron. Lett. **20**, 664 (1984).
[18] J. S. Barton and M. Saoudi, J. Phys. E: J. Sci. Instrum. **19**, 64 (1986).
[19] T. Nemoto, Y. Hashimoto, S. Sato, and H. Iitaka, Electr. Eng. Jpn. **125**, 1 (1998).
[20] S. Webstert, R. McBride, J. S. Barton, and J. D. C. Jones, Meas. Sci. Technol. **3**, 210 (1992).
[21] J. Lim, Q. P. Yang, B. E. Jones, and P. R. Jackson, Sens. Actuators, A **92**, 102 (2001).
[22] Y. Zhao, K. Chen, and J. Yang, Measurement **38**, 230 (2005).
[23] S. Takashima, H. Asanuma, and H. Niitsuma, Sens. Actuators, A **116**, 66 (2004).
[24] S. A. Wade, W. Jolley, and A. Fouras, Rev. Sci. Instrum. **79**, 065102 (2008).
[25] C. A. Wade and A. Dandridge, Electron. Lett. **24**, 783 (1988).
[26] R. P. Hu and X. G. Huang, IEEE Sens. J. **9**, 1952 (2009).
[27] R. Philip-Chandy, P. J. Scully, and R. Morgan, Meas. Sci. Technol. **11**, N31 (2000).
[28] J. Mireles, Jr., Sens. Rev. **25**, 33 (2005).
[29] V. Lien and F. Vollmer, Lab Chip **7**, 1352 (2007).
[30] P. Puangmali, K. Althoefer, and L. D. Seneviratne, IEEE Trans. Instrum. Meas. **59**, 283 (2010).
[31] Texas Advanced Optoelectronic Solutions, TAOS TSL1401R−LF datasheet, 2007.
[32] U. Frey, J. Stocks, A. Coates, P. Sly, and J. Bates, Eur. Respir. J. **16**, 731 (2000).
[33] J. M. Gere and B. J. Goodno, *Mechanics of Material*, 7th ed. (Cengage Learning, Toronto, 2009), pp. 305–337.
[34] F. Pigeon, S. Pelissier, A. Mure-Ravaud, H. Gagnaire, and C. Veillas, Electron. Lett. **28**, 1034 (1992).
[35] A. D. Yablon, *Optical Fiber Fusion Splicing* (Springer-Verlag, Berlin, 2005), p. 58.
[36] S. F. Hoerner, *Fluid-Dynamic Drag: Theoretical, Experimental and Statistical Information* (Hoerner Fluid Dynamics, 1965), pp. 3–17.
[37] D. L. A. Lisoski, Ph.D. dissertation, California Institute of Technology, Pasadena, 1993.
[38] Joint Committee for Guides in Metrology (JCGM), Evaluation of measurement data – Supplement 1 to the "Guide to the expression of uncertainty in measurement" – Propagation of distributions using a Monte Carlo Method, 101, 2008.
[39] Joint Committee for Guides in Metrology (JCGM), Evaluation of measurement data – Guide to the expression of uncertainty in measurement, 100, 2008.